FORSCHUNGSZENTRUM JÜLICH GmbH

Institut für Plasmaphysik
Association EURATOM-KFA

Single Projection Tomography in Plasma Physics

G. Fuchs V. Pickalov N. Preobrazhenski

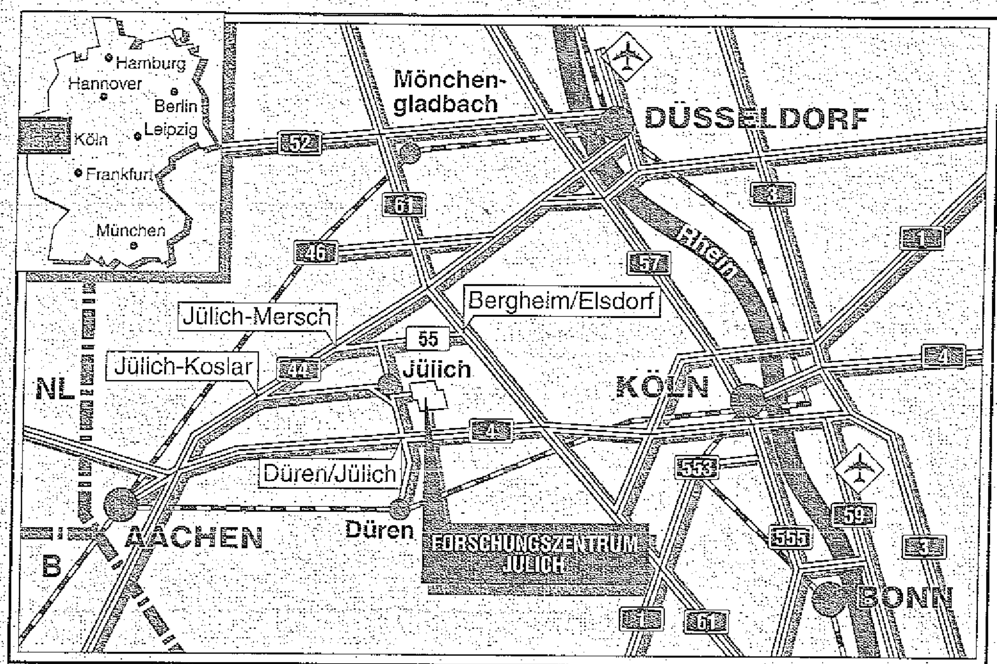

Berichte des Forschungszentrums Jülich ; 3014
ISSN 0944-2952
Institut für Plasmaphysik Jül-3014
Association EURATOM-KFA

Zu beziehen durch: Forschungszentrum Jülich GmbH · Zentralbibliothek
D-52425 Jülich · Bundesrepublik Deutschland
Telefon: 02461/61-6102 · Telefax: 02461/61-6103 · Telex: 833556-70 kfa d

Single Projection Tomography in Plasma Physics

G. Fuchs   V. Pickalov   N. Preobrazhenski

Single Projection Tomography in Plasma Physics

G. Fuchs, V. Pickalov[1] and N. Preobrazhenski[1]

Institut für Plasmaphysik KFA Jülich GmbH, Germany, Ass. EURATOM–KFA
[1]Institute of Theoretical and Applied Mechanics, Novosibirsk, Russia, Academy of Science

Abstract

In several practical applications, e.g. in plasma physics, one is confronted with the situation that only one viewing direction is available to collect data, which have to be inverted tomographically. We give analytic solution methods for special analytically known isocontours like concentric and non-concentric circles and ellipses as well as for some others. We also present a method to invert the data, when there is no analytic solution possible or when the isocontours are given numerically only.

1 Introduction

The literature on computerized tomography (CT) has been growing fast during the last two decades and many relevant theoretical and practical questions have been investigated (see [1]). Nevertheless, many important problems have been left aside. One of them being the proper choice of reconstruction algorithms more suitable for specific applications.
In comparing CT with other diagnostic methods, which are useful to study processes in plasmas, we may notice that the tomographic approach is especially efficient, when the full 2–D image of a plasma cross–section (sometimes it may even be 3–D) can be fast and reliably derived from a limited set of projections, which have been simultaneously (or almost simultaneously) measured. The over–all requirements for good algorithms are rather obvious. In particular they are:

- the stability of the reconstruction,
- an efficient sampling,
- the possibility to deal with a limited number of chords and projections,
- the treatment of noise on the measurements,
- good space resolution and accuracy and
- high speed of computation.

Additional requirements may include some generalizations of the standard CT problem like 3–D imaging using P (X–ray) or D (divergent beam) transforms [2], taking into account curvilinear beam trajectories, self–absorption of spectral lines, screening of a part of the beam etc. More special properties of an algorithm may be in connection with an emphasis on some typical details of the structure, with amplification of the image contrast etc.
As it is usual, CT algorithms may be divided into two groups:

- algebraic algorithms, i.e. such ones where the problem of reconstruction of the image from the projection is attacked by discretization right from the beginning and
- integral transform methods, which are based on some kind of analytic inversion formulas and which use discretization only, if it becomes necessary for numerical reasons.

Algebraic algorithms are more general, because they are closely and naturally connected with the modern optimization theory. On the other hand, integral transform methods are usually faster, perform better under standard conditions, and they can be better adapted to the intrinsic structures of the particular problem (e.g. isolines).
In the next section (2) we will begin our analysis with the simple situation, where the problem can be solved by Abel inversion. Nevertheless, some non–trivial approaches to inversion are discussed there. More sophisticated cases of non–concentric isolines, which usually involve two independent sets of projections are briefly described in section 3. Further complications due to moderate distortions of the isoline contours, which are, however, not so serious as to prevent 2–D reconstructions are discussed in section 4. As a result we get closer to the general tomographic problem solved on the base of more informative projection data.
In many cases encountered in plasma physics the access to the experiment is limited and the patterns to be recontructed change rapidly. However, there is usually additional information about the plasma from which it is sometimes possible to know the isocontour lines of the emission, e.g. magnetic surfaces are usually such isocontours. In section 5 we will treat the inversion for arbitrary but given isocontours.

2 Image Reconstruction from a Single Projection: Abel Inversion.

For the further analysis it is worthwhile to remember, first of all, several very simple results which apply to the case where the plasma **emissivity** $g(\vec{r})$ is a radially concentric function, i.e. $g(\vec{r}) = g_0(|\ \vec{r}\ |) \equiv g_0(r)$, consequently $f(\vec{p}) = f_0(|\ \vec{p}\ |) \equiv f_0(p)$, i.e. all **projections** $f(\vec{p})$ become equivalent and independent from the angular variables. For simplicity we deal here mainly with the 2–D case and keep in mind that the vector $\vec{r}$ and the vector for the impact parameters $\vec{p}$ (see [1, 2]) are given in the polar coordinate system: $\vec{r} = \vec{r}(r, \theta)$, $\vec{p} = \vec{p}(p, \varphi)$. It means, that in cartesian coordinates the integration may be performed for instance along the y–axis and

$$f_0(p) = f_0(x) = \int_{-\infty}^{\infty} g_0(r)\, dy = \int_{|x|}^{\infty} \frac{r g_0(r)}{\sqrt{r^2 - x^2}}\, dr \tag{1}$$

In other words one can say that the Radon transform is reduced to the Abel transform.

$$f_0(p) = \hat{R}\{g_0(r)\} = \hat{A}\{g_0(r)\} \tag{2}$$

One way to find the inversion formula is, to calculate the 2–D Fourier image of $g_0(r)$:

$$\begin{aligned} \hat{F}_2\{g(\vec{r})\} \equiv \tilde{g}(\vec{\xi}) &= \int_0^{\infty} r g_0(r) dr \int_0^{2\pi} e^{-2\pi i r \xi_r \cos\alpha}\, d\alpha \\ &= 2\pi \int_0^{\infty} r g_0(r) J_0(2\pi r \xi_r)\, dr = \hat{H}_0\{g_0(r)\} \end{aligned} \tag{3}$$

where $\tilde{}$ denotes the result of the Fourier transform by which the position vector $\vec{r}(r, \xi)$ transforms to the of space frequencies $\vec{\xi}(\xi_r, \xi_\theta)$, $\alpha = \xi_\theta - \theta$, J_0 is the Bessel function of zero order and $\hat{H}_0$ is the zero order Hankel transform.
Inversion of the equ.(3) is straight forward

$$\begin{aligned} g_0(r) &= \hat{F}_2^{-1}\{\tilde{g}(\vec{\xi})\} = 2\pi \int_0^{\infty} \xi_r \tilde{g}_0(\xi_r) J_0(2\pi r \xi_r)\, d\xi_r \\ &= \hat{H}_0\{\tilde{g}_0(\xi_r)\} = \hat{H}_0 \hat{F}_1\{f_0(x)\}, \end{aligned} \tag{4}$$

because the forward and inverse Hankel operators are identical.
The calculation of the fast Hankel transform is developed in detail in ref. [3, 4].
After some algebra, which is omitted here, the intermediate integral expression equ.(4) leads to the well–known formulae for the Abel inversion:

$$g_0(r) = -\frac{1}{\pi} \int_r^{\infty} \frac{f_0'(x)}{\sqrt{x^2 - r^2}}\, dx = -\frac{1}{\pi r} \frac{d}{dr} \int_r^{\infty} \frac{x f_0(x)}{\sqrt{x^2 - r^2}}\, dx \tag{5}$$

A large amount of literature is related to the various aspects of the Abel inversion and its applications to physics (see e.g. [5]). We emphasize here only three simple approaches which may be useful in processing data from plasma radiation.
1) Sometimes it is advantageous to reformulate the problem namely in cases where one is looking not for the radial function $g_0(r)$ itself, but for another function $\bar{g}_0(r)$ which is related to $g_0(r)$ via some physical process (see e.g. ref. [6, 7, 8]). For instance instead of equ.(5) one can write:

$$\bar{g}_0(r) = \frac{1}{2\Delta} \int_{r-\Delta}^{r+\Delta} g_0(\rho)\, d\rho = -\frac{1}{2\Delta} \int_{r-\Delta}^{r+\Delta} d\rho \int_{\rho}^{R} \frac{f_0'(x)}{\sqrt{x^2 - r^2}}\, dx \tag{6}$$

where $g_0(r)$ is averaged over a finite space interval 2Δ and Δ is defined by the degree of a priori information concerning the plasma diagnostic experiment, in particular by the noise level. In fact, the region of integration in equ.(6) is a trapezoid bound by the lines $x = \rho$ and $x = R$, $\rho = r \pm \Delta$, R is large enough. It is easy to see that the inverse problem in the form equ.(6) becomes well posed (stable) and the experimenter picks Δ either from the known error of the measurements or from the data of a real experiment.
2) Another approach uses the version of equ.(5) obtained after integration by parts again with the finite large upper limit R [9, 10]:

$$g_0(r) = \frac{1}{\pi}\left[\frac{f_0(R) - f_0(r)}{\sqrt{R^2 - r^2}} + \int_0^R \frac{x\,[f_0(x) - f_0(r)]}{(x^2 - r^2)^{3/2}}\,dx\right] \tag{7}$$

The absence of the derivative $f_0'(x)$ in this expression formally makes it stable, however, another problem arises, which is related to the undetermined integrand in the form $\frac{0}{0}$ when $x = r$. There is no sufficient base to use here the usual methods for numerical integration (e.g. three–point Gauss formula as proposed in ref.[9]). Nevertheless the indefinite character of equ.(7) can be overcome and the modern spline function technique can be used [10]. In many cases the computation using the formula equ.(7) is quite efficient.
At the end of this section we call attention to a simple and useful result related to a 3–D $g_0(r)$ depending on radius only. In a cartesian and sperical coordinates:

$$r^2 = x^2 + y^2 + z^2 \tag{8}$$

and the following formulae apply:

$$\begin{aligned} f_0(p) = f_0(x) = \hat{R}\{g_0(r)\} = \int_{-\infty}^{\infty} dy \int_{-\infty}^{\infty} g_0(r)\,dz, \\ \int_{-\infty}^{\infty} dy \int_{-\infty}^{\infty} dz = 2\pi \int_{-\infty}^{\infty} r\,dr, \end{aligned} \tag{9}$$

hence

$$f_0(x) = 2\pi \int_{|x|}^{\infty} r g_0(r)\,dr. \tag{10}$$

The necessary inversion formula follows at once as a result of differentiation [11]:

$$g_0(r) = -f_0'(r)/2\pi r \tag{11}$$

and the procedure of integration is not needed at all. So the reconstruction of the 3–D symmetrical image in the point r requires only the plane projection data in the vicinity of this point which is then sufficient for the calculation of $f'(r)$. This interesting result has been found as early as 1929 by J. Du Mond [13], however, it is not widely known.

3 Non–concentric Circular and Elliptical Isolines

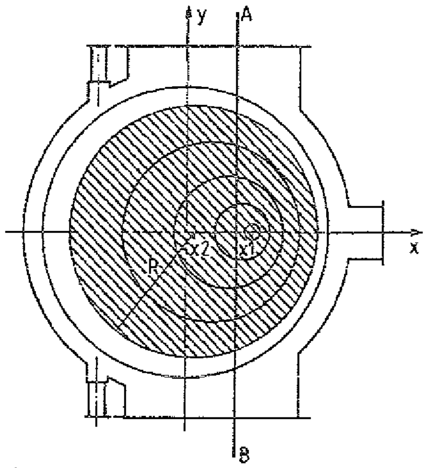

Figure 1: Plasma column with a set of shifted non–concentric isolines. The signal $f(x)$ is measured along the line A–B.

Plasma physicists often meet situations, where the assumption of concentric isolines is violated. Nevertheless some properties of symmetry apply (e.g. flux surfaces) and it pays to use them as a priori information rather than treating a general asymmetric case. In fig.1 the scheme of a rather typical case is plotted, where the plasma cross–section (hatched area with radius R) is shifted as a whole away from the centre of the vessel, which is indicated in fig.1 by the outer circle. The set of isolines then consists of a set of non–concentric circles shifted by a distance which depends on their radii. If this dependence on the radius is linear we can put

$$(x - x_1 + \kappa r)^2 + y^2 = r^2, \quad 0 \le r \le R, \quad \kappa \ge 0 \tag{12}$$

If the two orthogonal (in x and y) normalized projections are measured we get in one case an ordinary and in the other case a generalized forward Abel transform:

$$\begin{aligned} f(y) &= 2\int_{|y|}^{R} \frac{g(r)}{\sqrt{r^2 - y^2}} r\, dr \\ f(x) &= 2\int_{x(r)}^{R} \frac{[r(1-\kappa^2) - \kappa(x - x_1)]\, g(r)}{\sqrt{r^2(1-\kappa^2) - 2\kappa r(x - x_1) - (x - x_1)^2}}\, dr \end{aligned} \tag{13}$$

where $x(r)$ is the positive root of the denominator and the condition $x_1 = \kappa = 0$ corresponds to the Abel case. In fact in the expression of the projection $f(x)$ two independent Volterra integral equations of 1^{st} kind are joint: one is related to the interval $x_2 - R \le x \le x_1$ and the other to the interval $x_1 \le x \le x_2 + R$. Thus by measuring two projections $f(y)$ and $f(x)$ we get three integral equations, two of them containing shift parameters x_1 and κ which are found in the process of joining the three solutions of equ.(13). As a result the isoline structure of the plasma can be obtained [1, 14].

These results can be generalized if one drops the assumption of linearity of the shift. A rather simple approach has been used by T. Takeda [15] and the more general analysis is given in ref.[12]. Instead of equ.(12) we may write

$$[x - \gamma(g)]^2 + y^2 = r^2(g) \tag{14}$$

considering the shift γ of each isoline along the x axis and its radius as some functionals of the unknown distribution $g(r)$. After some algebra we get for the projection $f(x)$ the following nonlinear integral equation related to the functionals $\gamma(g)$, $r(g)$ and their first derivatives:

$$\begin{aligned}
\gamma'(g) &= \frac{d\gamma(g)}{dg}, \quad r'(g) = \frac{dr(g)}{dg} \\
f(x) &= \int_{g(x-\gamma)}^{0} \frac{r(g) - [\gamma(g) - r(g)]\,\gamma'(g)}{\sqrt{r^2(g) - [x - \gamma(g)]^2}} g r'(g)\, dg,
\end{aligned} \tag{15}$$

For $\gamma(g) \to 0$ (20) becomes

$$f(x) = \int_{g(x)}^{g(R)} \frac{\frac{d}{dg} r^2(g)}{\sqrt{r^2(g) - x^2}} g\, dg, \tag{16}$$

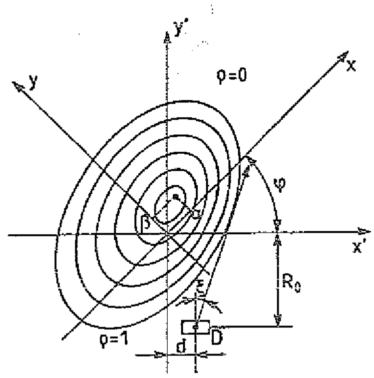

Figure 2: A set of shifted elliptical isolines with a fan beam detector D. ξ being the scanning angle.

which is equivalent to the Abel transform, when $f(x) = f(y)$, $f(y)$being given by the first equation of equ.(13).

T.Takeda [15] used this simplified nonlinear approach (with the additional assumption of a monotonic decrease of g(r) from the center to the periphery of the plasma) and tried to reconstruct the electron density profile in JFT–2 tokamak plasma. However, the regularization given in [15] was insufficient and the artifacts were too large.

Another example is a plasma column with regularly shifted elliptical isolines, fig.2 [17]. Note, that E. Silver and W. Roney [18] who published their results one year later studied a similar problem, however, with more stringent limitations. Elliptical isolines satisfy the equation

$$\frac{[x - A(\rho)]^2}{a^2} + \frac{[y - B(\rho)]^2}{b^2} = \rho^2 \tag{17}$$

where a and b are the half–axes of an ellipses, ρ is the generalized radial variable changing from $\rho = 1$ (external ellipse) to $\rho = 0$ (the "bunching point" (α, β)). Equ.(17) is written in the coordinate system XOY rotated with respect to the laboratory frame $X'OY'$ by the angle φ; d is a shift of the detector D viewing a fan–beam. In the linear case we have:

$$A(\rho) = \alpha(1 - \rho), B(\rho) = \beta(1 - \rho) \tag{18}$$

and for the fan–beam projections $f(\xi)$ (see fig.2) we obtain

$$f(\xi) = \int_{\rho_1}^{1} K(\rho, \xi) g(\rho)\, d\rho, \tag{19}$$

where [1]

$$\begin{aligned}
K(\rho,\xi) &= \frac{2ab}{m^2} \times \frac{\rho(m^2-\gamma^2)+\gamma(\gamma-R_\xi \sin\xi)}{\sqrt{(m^2-\gamma^2)(\rho-\rho_1)(\rho+\rho_2)}} \\
m^2 &= a^2\cos^2(\varphi+\xi)+b^2\sin^2(\varphi+\xi), \\
\gamma &= \alpha\cos(\varphi+\xi)-\beta\sin(\varphi+\xi), \\
R_\xi &= R_0 + d\cot\xi, \\
\rho_1 &= \mid \gamma - R_\xi \sin\xi \mid /(m\mp\gamma), \\
\rho_2 &= \mid \gamma - R_\xi \sin\xi \mid /(m\pm\gamma).
\end{aligned} \tag{20}$$

In the expressions for ρ_1 and ρ_2 the upper signs relate to the chords on the right side of the "bunching point", and vice versa. Note, that we present here a somewhat more general case as compared to the one in ref.[17], where there was no shift of the external ellipse, i.e. $d = 0$. As in [18] it corresponds to the more special case of the absence of any internal shifts of the ellipses: $\alpha = \beta = 0$.
A transition from the fan–beam to the parallel beam scanning makes the problem notably simpler. Formally it means a change of variables

$$R_\xi \sin\xi \to x, \quad (\varphi+\xi)\to\theta \tag{21}$$

where θ is now the angle of rotation of the external ellipse relative to the laboratory frame. Instead of equ.(19) and equ.(20) we obtain

$$f(x) = \int_{\rho_1}^{1} K(\rho,x)g(\rho)\,d\rho \tag{22}$$

where

$$\begin{aligned}
K(\rho,x) &= \frac{2ab}{m^2} \times \frac{\rho(m^2-\gamma^2)+\gamma(\gamma-x)}{\sqrt{(m^2-\gamma^2)(\rho-\rho_1)(\rho+\rho_2)}} \\
m^2 &= a^2\cos^2\theta+b^2\sin^2\theta, \quad \gamma=\alpha\cos\theta-\beta\sin\theta, \\
\rho_1 &= \mid \gamma - x \mid /(m\mp\gamma), \quad \rho_2 = \mid \gamma - x \mid /(m\pm\gamma).
\end{aligned} \tag{23}$$

Real projection data from a low temperature plasma in a longitudinal magnetic field were used for tomographic reconstruction in ref.[19]. The spiral form of the plasma column allowed to use elliptical isolines as a model together with $\beta = \theta = 0$, which then considerably simplifies the kernel of the integral equ.(22):

$$\begin{aligned}
K(\rho,x) &= \frac{2b}{a} \times \frac{\rho(a^2-\alpha^2)+\alpha(\alpha-x)}{\sqrt{(a^2-\alpha^2)(\rho-\rho_1)(\rho+\rho_2)}} \\
\rho_1 &= \frac{x-\alpha}{a-\alpha}, \quad \rho_2=\frac{x-\alpha}{a+\alpha}, \quad m=a, \quad \gamma=\alpha, \quad x\ge a.
\end{aligned} \tag{24}$$

Equ.(22) was again solved with the method of statistical regularization which guaranteed a stable solution with a small (order of one) coefficient of the error amplification: σ_g/σ_f where σ_g and σ_f are the dispersions of the emissivities and of the projection data respectively. The experiment [19] opened the interesting possibility to evaluate the role of different numbers of views. In some interval of magnetic field strength the scheme of elliptic isolines has been proven to be successful, hence only two projections $f(x)$, $f(y)$ were needed. However, with increasing magnetic field the plasma became more asymmetric and a satisfactory reconstruction required more projections, in the concrete case the number of projections had to be at least six. A rather smooth transition from a special to a general 2–D tomographic problem was observed.
In conclusion for this section some important special cases for elliptical geometry are mentioned:
a) If $a = b = 1$ and the shift of isolines occurs along x only, we obtain instead of the formulae equ.(22) and equ.(23) the above formulae equ.(12) and equ.(13) for a system of non–concentric circles as isolines.
b) Another special case is given when $\alpha = \beta = \theta = \gamma = 0$, $a = b = m = 1$, $\rho = r$, $\rho_1 = \rho_2 = x$ then we obtain a simple Abel equation determined in the unit circle

$$f(x) = 2\int_x^1 \frac{rg(r)}{\sqrt{r^2 - x^2}}\, dr \tag{25}$$

c) Accepting $a = \alpha$ in the kernel, we come again to the Abel equation written in a slightly modified form:

$$f(x) = 2b\sqrt{z_1}\int_{z_1}^1 \frac{g(\rho)}{\sqrt{\rho - z_1}}\, d\rho, \quad z_1 = \frac{a - x}{2a}. \tag{26}$$

In case of fan–beam scanning the degeneracy of the problem is connected with the condition

$$m = \alpha\cos(\varphi + \xi) \tag{27}$$

and again we get an equation similar to equ.(26)

$$f(\xi) = \frac{2ab}{m}\sqrt{z_2}\int_{z_2}^1 \frac{g(\rho)}{\sqrt{\rho - z_2}}\, d\rho, \quad z_2 = \frac{m - R_\xi \sin\xi}{2m}. \tag{28}$$

d) Neglecting shifts and rotations of elliptical isolines but taking into account higher indices $n \geq 1$ gives [1]:

$$\left(\frac{x^2}{a^2}\right)^n + \left(\frac{y^2}{b^2}\right)^n = \rho^{2n}, \quad \rho \in [0,1],$$
$$f(x) = 2b\int_{x/a}^1 \frac{\rho^{2n-1}g(\rho)}{[\rho^{2n} - (x/a)^{2n}]^k}\, d\rho,$$
$$k = (2n-1)/2n, \quad k \in [0.5, 1), \quad n \geq 1 \tag{29}$$

which after the substitution

$$\rho^{2n} = 1 - u; \quad (x/a)^{2n} = 1 - v \tag{30}$$

leads to the ordinary form of the Abel transform,

$$g(\rho) = -\frac{n\sin(k\pi)}{2\pi k} \cdot \int_\rho^1 \frac{f'(x)dx}{[(x/a)^{2n} - \rho^{2n}]^{1-k}}. \tag{31}$$

4 Sets of Disturbed Isolines

The idea here is to restore a moderately distorted 2–D plasma distribution $g(\vec{r})$ by two orthogonal projections $f(x)$ and $f(y)$ and with the representation of $g(r,\theta)$ by three leading terms in a Fourier expansion [1, 21, 22]:

$$g(\vec{r}) = g(r,\theta) = g_0(r) + g_1(r)\cos\theta + g_2(r)\sin\theta \tag{32}$$

where g_0, g_1, g_2 are restricted only in the sense that they are well behaved functions of the radius.

Each of the projections can be decomposed into symmetric and antisymmetric parts in such a way:

$$\begin{aligned}
f_1(x) &= [f(x) - f(-x)]/2x, \\
f_1(y) &= [f(y) - f(-y)]/2y, \\
f_2(x) &= [f(x) + f(-x)]/2, \\
f_2(y) &= [f(y) + f(-y)]/2.
\end{aligned} \tag{33}$$

In order to keep the following expressions short, it is convenient to use a functional [1]

$$A(\psi; u - v) \equiv \frac{\psi(u)u}{\sqrt{u^2 - v^2}} \tag{34}$$

where ψ is some arbitrary but well behaved function and $0 \le u, v \le R$. Of course it is easy to see the origin of $A()$ from the Abel transform. After some algebra one obtains

$$\begin{aligned}
f_1(x) &= 2\int_x^R A(g_1/r; r - x)\,dr, \\
f_1(y) &= 2\int_y^R A(g_2/r; r - y)\,dr, \\
f_2(x) &= 2\int_x^R A(g_0; r - x)\,dr, \\
f_2(y) &= 2\int_y^R A(g_0; r - y)\,dr
\end{aligned} \tag{35}$$

The effect of data "abundance" due to the possibility of finding the radial function $g_0(r)$ from any of the two last equations (33) is very useful in practice because it helps to diminish the error of reconstruction due to an inaccurate choice of the center of the column (see for details ref.[1]).
K.Lapworth and L.Allnut [22] who studied spectroscopically the temperature fields in HF–discharges in argon showed that their case of inhomogeneities was simple enough to be of interest fairly well by reconstruction similar to equ.(32). Applying rather cumbersome techniques for successive Abel inversion which in fact is equivalent to equ.(33) these authors found that the error of temperature reconstruction was about 1% and the error of local emissivity reconstruction was approximately 7%. Similar work has been done for tokamaks by [20].

5 General isolines

The methods presented so far deal with isolines represented by a set of closed and nested lines of special shape – in the most simple case concentric circles. If a continuous mapping of the set of nested circles can be found one may generalize the case to known but otherwise arbitrary isolines of emission, a necessary condition being that the emission function does not contain saddle points, i.e. the isolines do not have x–points.
Let's suppose that such a mapping were possible and that the isolines are given by a function $\Psi(x, y)$, in the x, y plane, i.e. $g = g(\Psi)$. In order to be able to locate each point in the plane we may choose another coordinate $\theta(x, y)$. In these coordinates a set of curves of sight, which need not be straight lines, can be described by a function $\theta(\Psi, p)$, where p is a parameter.
Knowing the transform $\{x, y\} \rightarrow \{\Psi, \theta\}$ we can calculate the components of the metric tensor G. The line element for the integration is then given by

$$ds = \sqrt{G}\, d\Psi\, d\theta \tag{36}$$

Along a line of sight G, Ψ and θ are functions of the impact parameter p, an angle ξ and the length s along the line. The line integral is then given by

$$f(p, \xi) = \int g(\Psi(p, \xi, s), \theta(p, \xi, s))K(\Psi(p, \xi, s), \theta(p, \xi, s))\, ds, \tag{37}$$

where the kernal K has to be calulated from the above line elememt. If the isocontours are known, a one–parametric set of lines of sight – e.g. a set of parallel beams or a fan beam – is sufficient for reconstruction, this even works, if the function g has more than one

extremum.
Equ.(37) is the simplified to the form:

$$f(p) = \int_L g(\Psi) K(p, \Psi)\, d\Psi. \tag{38}$$

In case the isolines are concave the value Ψ along the lines of sight is bivalued, which can be taken care of by use of a kernal of the form:

$$K(p, \Psi) = Q^+(p, \Psi) - Q^-(p, \Psi), \tag{39}$$

whereby the functions Q are like those in the example of fig.3, i.e. there are poles where the lines of sight are tangent to a isoline. If the function $g(\Psi)$ has more than one maximum, equ.(39) has to be replaced by

$$K(p, \Psi) = \sum_{i(p)} Q^+(p, \Psi) - Q^-(p, \Psi), \tag{40}$$

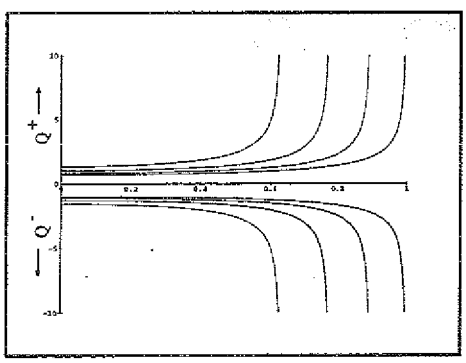

Figure 3: An example for a bivalued kernal cf. equ.(38)

where i is the number of maxima (or minima) visited along a line of sight.
In practice we may procede as follows:
We introduce a normalized isoline label $\rho \in [0, 1]$ and an equispaced grid on it with $(N_\rho - 1)$ intervals and as result we have an equispaced grid for $\Psi \in [\Psi_{min}, \Psi_{max}]$. Then we construct a one-dimensional grid function $\Psi(l_i), i = 1, \ldots, N_b$ for the ray L by using a two-dimensional interpolation (e.g. a bi-linear one). Let dl_p be the path differential, then we have

$$f(p) = \int g(l)\, dl_p = \int g(\rho) \left(\frac{dl_p}{d\rho}\right) d\rho. \tag{41}$$

The grid of the $\{l_i\}$ we divide into intervals with monotonically varying functions $\Psi(l_i)$; the number q of such intervals is even. For each interval we determine functions $l_i^{(q)} = l(\Psi_i)$, and therefore after the transformation $\Psi_i \to \rho_i$ we have grid functions $l_i^{(q)} = l(\rho_i), i = 1, \ldots, N_b$. Using smooth approximation of each function $l_i^{(q)}$ (e.g. with cubic splines) we determine derivatives of l_p for (41). So the final formula for the described algorithm is [1]:

$$f(p) = \int_0^1 \left[\sum_{j=1}^{q} \eta_j^p \left| \frac{dS^{(j)}(\rho)}{d\rho} \right| \right] g(\rho)\, d\rho, \tag{42}$$

$$\eta_j^p = \begin{cases} 0, & \rho < \rho_{0j}, \\ 1, & \rho \geq \rho_{0j}. \end{cases}$$

Here $S^{(j)}$ is a cubic spline for the j^{th} interval, and ρ_{0j} are values for the local maxima of $\Psi(l_j)$. For a numerical realization of this algorithm we need to exclude a singularity in the point ρ_{0j}, to make – after the regularization of the integral – the equation to be of Volterra type of first kind, to do the two–dimensional interpolation of $\Psi(x, y)$ and to reverse $\{g_i\}$ to $g(x_i, y_i)$. Depending on the shapes of the isolines, there may or may not be an analytic solution of the problem to resolve for g [1].
An example is given in fig.4. In the numerical simulations we have checked the properties of statistical regularization methods (Bayesian approach from [16]) as applied to the solution of the integral equation of Volterra first kind.

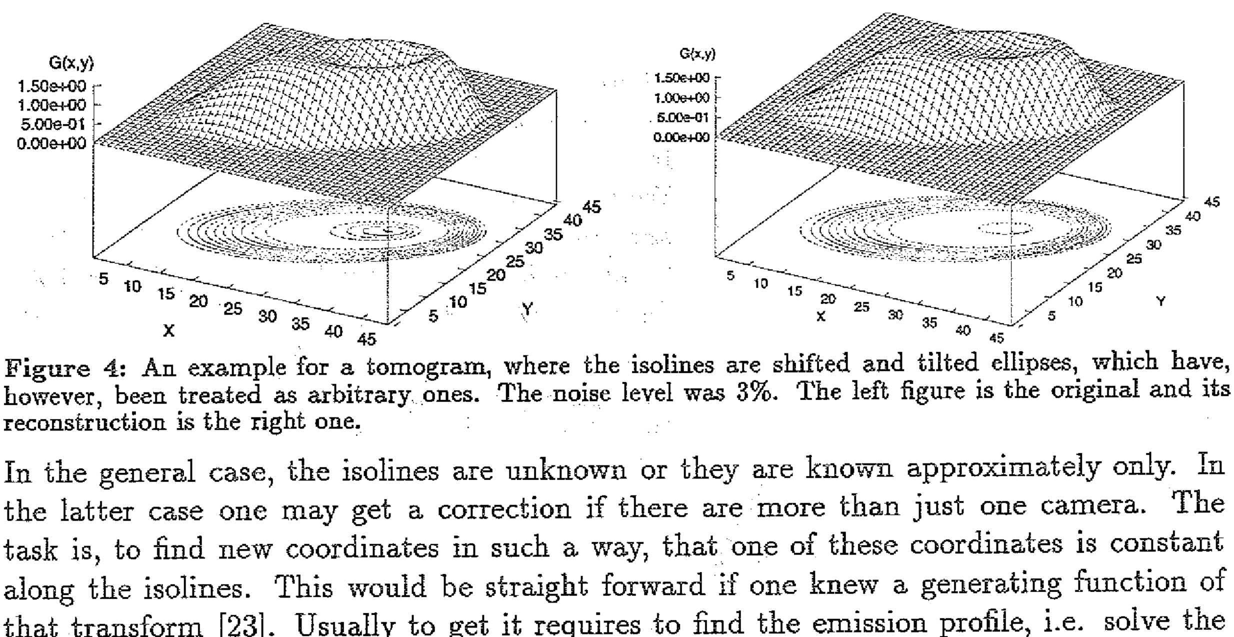

Figure 4: An example for a tomogram, where the isolines are shifted and tilted ellipses, which have, however, been treated as arbitrary ones. The noise level was 3%. The left figure is the original and its reconstruction is the right one.

In the general case, the isolines are unknown or they are known approximately only. In the latter case one may get a correction if there are more than just one camera. The task is, to find new coordinates in such a way, that one of these coordinates is constant along the isolines. This would be straight forward if one knew a generating function of that transform [23]. Usually to get it requires to find the emission profile, i.e. solve the inversion problem. This may nevertheless be rewarding if one deals with profiles, which change in time, whereby, however, the isolines do not, a case which applies e.g. to the profiles of various plasma parameters during sawtoothing in tokamaks.

6 Conclusion

For many practical applications of tomography one has to deal with situations, where there are only a few line integrated data available over a cross section, and they may also belong

to one viewing direction or one fan beam only. From these limited data local emission has to be derived. This kind of problem is e.g. often faced in plasma physics, where the access to the experiments is rather limited and has to be shared with many other diagnostics so that only one camera may be available. Usually it cannot be assumed, that the local emission is axisymmetric and allows Abel inversion.
One may, however, have information about the shape of the isolines from other diagnostics or from theory, e.g. transport and equilibrium code calculations. It is shown in the paper, that one can either taylor an inversion formula for the particular case and solve in this manner analytically, or one can find a numerical solution. In both cases we give methods to find the kernal of the integral equation and solve the inversion problem.
In many experimental situations, although there is only a limited amount of data in space there may be a lot of information on the time evolution. Again, if there is information on the dynamics of the system, this method may be extended to study this dynamics. In future we intend to procede along this way.

Acknowledgments

It is a pleasure of one of the authors (N. Preobrazhensky) to thank Prof. E. Hintz for his kind invitation to IPP, KFA, Jülich and support for further cooperation in the field of plasma tomography. This work has been founded by the Deutsche Forschungsgemeinschaft and the Russian Academy of Sciences.

References

[1] Pickalov V.V., Preobrazhensky N.G., Reconstructive Tomography in Gas Dynamics and Plasma Physics, Novosibirsk; Nauka 1987 (in Russian)

[2] Natterer F., The Mathematics of Computerized Tomography, Stuttgart: B.G. Teubner, 1986

[3] Anderson W.L., Computer program: numerical integration of related Hankel transforms of orders 0 and 1 by adaptive digital filtering, Geophysics, 1979-V.44.No 7-p.1287-1305

[4] Bisseling R., Kosloff R., The fast Hankel transform as a tool in the solution of the time dependent Schrödinger equation, J. Comput. Phys.-1985-V59, No 1-p.136-151

[5] Abel Inversion and Its Generalizations, ed. N. Preobrazhensky, Novosibirsk: Institute of Theoretical and Applied Mechanics, Russian Acad. Sci., 1978

[6] Preobrazhensky N.G. Pickalov V.V., Unstable Problems of Plasma Diagnostics, Novosibirsk: Nauka, 1982 (in Russian)

[7] Luizova L.A., Physically based regularization technique in the problem of radial transform, Optics and Spectroscopy - 1982 - V.52, No 4-p.690-695

[8] Frank A.G., et al., Spectroctomography of current sheet plasma in nonlinear regime of magnetic reconnection - In: ICPIG-XIX, Contributed Papers, Belgrade, 1989-P.740-741

[9] Deutsch M., Beniaminy I., Derivative-free inversion of Abel's integral equation, Appl. Phys. Lett., 1982-V.41, No 1-p.27-28

[10] Voskoboinikov Ju.E., Preobrazhensky N.G., Abel inversion with improved accuracy in the problems of optics and spectroscopy, Optics and Spectroscopy, 1986-V.60, No 1-p.179-183

[11] Barrett H.H. The Radon transform and its applications. Ch.III in: Progress in Optics, Ed.E.Wolf, Elsevier, Amsterdam, 1984, p. 218 - 286.

[12] Preobrazhensky N.G., New trends for development of integral transform methods in computerized tomography, - In: Ill-Posed Problems, The 1st Internat. Conf., Moscow, 1991, Book of Abstracts, p. 218

[13] Du Mond J.W.M., Compton modified line structure and its relation to the electron theory of solid bodies, Phys. Rev. - 1929 - V.33-p.643-647

[14] Gorbunov E.P., et al., Determination of plasma density distribution by phase shift in multichannel wave probing - In: Plasma Diagnostics, V.2, Moscow, Atomizdat, 1968, p.188-199 (in Russian)

[15] Takeda T., Numerical method for solution of the integral equation of the first kind - application to analysis of plasma density profile, J. Comput. Phys. - 1976 - V.21, No 3-p.305-318

[16] Turchin V.F., Kozlov V.P., Malkevich, M.S., The use of mathematical-statistics methods in the solution of incorrectly posed problems, Soviet Physics, Uspekhi, 1971-V.13, No 6-p.681-703

[17] Pickalov V.V., Preobrazhensky N.G., Local diagnostics of gaseous and plasma objects with known isolines, Optics and Spectroscopy-1979-V.46, N1-P.194-196

[18] Silver E., Roney W., Distribution of emitters in an elliptical source, IEEE Trans. Plasma Science - 1980-V.PS-8, No 3-p.231-234

[19] Melnikova T.S., Pickalov V.V., Preobrazhensky, N.G., On the local diagnostics of the optically thick asymmetric plasma, Optics and Spectroscopy - 1980 - V.48,No 3-p.474-479

[20] Nagayama Y., Edwards A.W., Rotational soft x–ray tomography of noncircular tokamak plasmas, Rev. Sci. Inst. 1992 V.63 No 10 p.4757–4759

[21] Freeman M.P., Katz S., Determination of a radiance–coefficient profile from the observed asymmetric radiance distribution of an optically thin radiating medium. J. Opt. Soc. Amer. 1963 V.53 p. 1172–1179

[22] Lapworth K.G., Allnutt L.A., A fully automatic optical system for determining the volume emission coefficient of radiation throughout plasmas. J. Phys. E: Sci. Instr., 1977 V–10 p. 727–732

[23] Fuchs G., Miura Y. and Mori M., Soft x–ray tomography in tokamaks using flux coordinates, Plasma Physics and Controlled Nuclear Fusion, 1994, V.36,p.307–316

FORSCHUNGSZENTRUM JÜLICH GmbH

Jül-3014
January 1995
ISSN 0944-2952